Flight Effects on Noise from Coaxial Dual Flow Part II: Heated Jets

R. Dash*
NASA Ames Research Center, Moffett Field, California

This paper is a continuation of the study described in Part I and deals with the flight effects on noise from heated jets. The present work shows that coaxial exhaust flows with inverted profiles are much quieter than flows with conventional profiles. Among all possible coaxial configurations with only one of the streams heated—conventional profile, inverted profile, and the variable stream control engine (VSCE) cycle—and holding constant mass flow and thrust, a VSCE cycle is the best possible engine cycle as it provides over 18-dB reduction in sound pressure level (as compared to noise from a conventional profile cycle) at all angles, both statically and in flight. The study also indicates that, if both the coaxial streams are heated unequally, a duct-burning profile, combined with the variable stream control engine (DB-VSCE) concept, gives rise to a powerful coaxial device which generates the least noise, both statically and in flight. This concept will be of paramount importance as one of the most variable nozzle designs of the future.

Nomenclature

c = speed of sound
d = diameter of the inner nozzle
D = diameter of the outer nozzle
I = intensity of radiation
k = wave number
K = propagation constant
M = Mach number of the jet flow
$\bar{M}$ = U_m/c_0
M_c = Mach number of source convection in the primary flow, U_c/c_0
$\mathfrak{M}_c$ = Mach number of source convection in the secondary flow, $\mathfrak{U}_c/c_0$
m = periodicity of the source in the primary flow
n = periodicity of the source in the secondary flow
p = acoustic pressure
q_m = strength of the ring source in the primary flow
q_n = strength of the ring source in the secondary flow
r = axial distance in the radial direction
r_p = radius of the primary flow
r_s = radius of the secondary flow
r_0 = axial distance of the ring source in the primary flow
$\mathfrak{r}_0$ = axial distance of the ring source in the secondary flow
R = distance between the source (in the primary flow) and the observer
$\mathfrak{R}$ = distance between the source (in the secondary flow) and the observer
St_1 = Strouhal number associated with source in the primary flow
St_2 = Strouhal number associated with source in the secondary flow
U = velocity of the jet flow
U_c = convection velocity of the source in the primary flow
$\mathfrak{U}_c$ = convection velocity of the source in the secondary flow
U_m = characteristic mean velocity
w = frequency of the source in the secondary flow
Γ = U_s/U_p
θ = angle of emission relative to the jet axis (at the retarded time)
ρ = density
Σ = outer-to-inner area ratio
ω = frequency of the source in the primary flow

Subscripts

f = conditions pertaining to flight
p = conditions in the primary flow
s = conditions in the secondary flow
rcp = conditions due to a ring source in the cold primary flow
rcs = conditions due to a ring source in the cold secondary flow
rhp = conditions due to a ring source in the hot primary flow
rhs = conditions due to a ring source in the hot secondary flow
0 = ambient conditions

Received Nov. 20, 1984; revision received Aug. 3, 1985. This paper is declared a work of the U.S. Government and is not subject to copyright protection in the United States.

*NRC-NASA Senior Research Associate; presently, Senior Acoustics Engineer, Douglas Aircraft Company, Long Beach, CA. Member AIAA.

Introduction

MODERN aeroengines produce coaxial jet flows that are unequally heated and characterized by density and temperature gradients across their flow interfaces. These interfaces exist at the boundaries of the primary and secondary flows, and secondary and ambient flows. While the noise prediction aspects of single round jets, both cold and hot, have been treated satisfactorily, Mani[1,2] has provided the most recent and complete treatment. He found that the jet mean flow has a profound effect on the production of far-field noise; adequate theoretical explaination and prediction of noise of coaxial round jets have, to that extent, been lacking. As an extension of Mani's approach to single round jets, a model of the aeroacoustic characteristics of coaxial round jets in flight is developed. Cold coaxial jets were treated in Part I[5]; however, most practical coaxial jets are not cold, they are the ones with both streams unequally heated. Thus, it is desirable to extend this model to develop an analytical tool for the prediction of noise from these coaxial, heated, round jets in flight.

Intrinsically Generated Extraneous Sources

The role played by the multipole sources in a heated jet is quite intricate and is difficult to explain through the physics

of the problem. To explain this, one can make use of the generalized properties of the delta function and its derivatives to show that, in the presence of two or more different fluid media having nonidentical temperatures and densities at their common interface, a dipole source term may give rise to an additional simple source term, and a quadrupole term may give rise to an additional dipole term plus one additional simple source term. Mani[1,2] has utilized this idea to solve the vortex-sheet modeling problem of the single, round, plug-flow jets. Since ours is a heated coaxial dual jet having double vortex layers, it will be worthwhile to show that by utilizing the delta function technique, one can find additional dipole and simple source terms generated from the quadrupole-type ring sources. The generation of these additonal source terms must be considered before one derives the final radiation from the heated coaxial flow through the ring modeling. The equations governing the wave propagation from the coaxial jets in flight are given in Part I.[5]

Before we explain mathematically how the additional source terms are intrinsically generated within the system, let us consider the multiplication property of the derivatives of generalized functions in conjunction with another fixed function which has continuous derivatives at least up to the nth order in a neighborhood of the origin (see Ref. 3),

$$\phi(\tau)\delta^n(\tau)=\phi(0)\delta^n(\tau)-{}^nC_1\phi'(0)\delta^{n-1}(\tau)$$
$$+{}^nC_2\phi''(0)\delta^{n-2}(\tau)-\ldots+(-1)^n\phi^n(0)\delta(\tau) \tag{1}$$

The dashes denote the differentiation with respect to the argument. Making use of this relation, one can write the a_{11}-quadrupole component of the source term as

$$a_{11}=\rho_s(r)\frac{\partial^2}{\partial x^2}\left\{\frac{\delta(r-r_0)}{r}\delta(z-U_c t)e^{-iwt}\right\}$$
$$=\rho_s(r_0)\left(\frac{\partial^2}{\partial x^2}\delta_s\right)-2\left(\frac{\partial\rho_s(r)}{\partial x}\right)_{r_0,\phi}\left(\frac{\partial\delta_s}{\partial x}\right)+\left(\frac{\partial^2\rho_s(r)}{\partial x^2}\right)_{r_0,\phi}\delta_s \tag{2a}$$

$$\delta_s=\frac{\delta(r-r_0)}{r}\delta(z-U_c t)e^{-iwt} \tag{2b}$$

In Eqs. (2), the differentiations are evaluated at $r=r_0$. The development of Eq. (2a) from its preceding step has been made possible by the presence of density gradients across the fluid interface at $r=r_s$ which separates the secondary stream from the ambient flow used to simulate flight. It is well known that the noise sources are principally generated in and around the secondary/ambient interface, although for the sake of convenience we replace them by a ring source in the secondary stream at $r=r_0$. Thus, the density gradients suffixed with r_0 essentially reflect the density gradients at $r=r_s$ where they really exist. We will come to this point again at a later stage. Making use of Eqs. (2) and following a similar procedure, we can write explicit expressions for all of the quadrupole components as

$$a_{11}=\cos^2\phi\left[\rho_s(r_0)\left(\frac{\partial^2\delta_s}{\partial r^2}\right)_{r_0}-2\rho_s'(r_0)\left(\frac{\partial\delta_s}{\partial r}\right)_{r_0}+\rho_s''(r_0)\delta_s\right]$$
$$+\frac{\sin^2\phi}{r_0}\left[\rho_s(r_0)\left(\frac{\partial\delta_s}{\partial r}\right)_{r_0}+\rho_s'(r_0)\delta_s\right] \tag{3a}$$

$$a_{22}=\sin^2\phi\left[\rho_s(r_0)\left(\frac{\partial^2\delta_s}{\partial r^2}\right)_{r_0}-2\rho_s'(r_0)\left(\frac{\partial\delta_s}{\partial r}\right)_{r_0}+\rho_s''(r_0)\delta_s\right]$$
$$+\frac{\cos^2\phi}{r_0}\left[\rho_s(r_0)\left(\frac{\partial\delta_s}{\partial r}\right)_{r_0}+\rho_s'(r_0)\delta_s\right] \tag{3b}$$

$$a_{33}=\rho_s(r_0)\frac{\partial^2\delta_s}{\partial z^2} \tag{3c}$$

$$a_{12}=\frac{\sin2\phi}{2}\rho_s(r_0)\left[\left(\frac{\partial^2\delta_s}{\partial r^2}\right)_{r_0}-\frac{1}{r_0}\left(\frac{\partial\delta_s}{\partial r}\right)_{r_0}\right]$$
$$-\sin2\phi\rho_s'(r_0)\left(\frac{\partial\delta_s}{\partial r}\right)_{r_0}+\frac{\sin2\phi}{2}\left[\rho_s''(r_0)-\frac{1}{r_0}\rho_s'(r_0)\right]\delta_s \tag{3d}$$

$$a_{13}=\cos\phi\left[\rho_s(r_0)\left(\frac{\partial^2\delta_s}{\partial r\partial z}\right)_{r_0}-\rho_s'(r_0)\frac{\partial\delta_s}{\partial z}\right] \tag{3e}$$

$$a_{23}=\sin\phi\left[\rho_s(r_0)\left(\frac{\partial^2\delta_s}{\partial r\partial z}\right)_{r_0}-\rho_s'(r_0)\frac{\partial\delta_s}{\partial z}\right] \tag{3f}$$

Equations (2) show that the a_{11} quadrupole resolves into a purely quadrupole term proportional to the local density of the stream, plus one transverse dipole term proportional to the local density gradient, and one simple source term proportional to the second-order local density gradient. However, when the a_{11} quadrupole is expressed in terms of polar coordinates, the scenario looks different. Similar interpretation can be provided for the a_{22} quadrupole in Eq. (3b). The purely axial a_{33} quadrupole remains unaffected and generates no lower order singularities because of the absence of any mean density gradient in the axial direction. The a_{12} quadrupole provides one radial quadrupole proportional to $\rho_s(r_0)\sin\phi\cos\phi$, plus one radial dipole term proportional to $\sin2\phi\{-[\rho_s(r_0)/(2r_0)]-\rho_s'(r_0)\}$, and one simple source term proportional to $\sin\phi\cos\phi\{\rho_s''(r_0)-[\rho_s'(r_0)/r_0]\}$. The a_{13} quadrupole provides one quadrupole proportional to $\rho_s(r_0)\cos\phi$ and one axial-type dipole proportional to $-\rho_s'(r_0)\cos\phi$. Similar interpretation follows for the a_{23} quadrupole. Now, following Mani's approach[2] for noise from single, heated, round jets, and recognizing the fact that the density gradients at $r=r_0$ really mean the density gradients across the fluid interface at $r=r_s$, where they physically exist, the density gradients can be expressed as

$$\rho_s'(r_0)=\frac{\rho_f-\rho_s}{r_s}St_2,\quad \rho_s''(r_0)=\frac{\rho_f-\rho_s}{r_s^2}St_2^2 \tag{4}$$

These Strouhal-number dependencies of the density gradients are discussed in Ref. 2. Following the same procedure, we can derive parallel expressions for the quadrupole components of the ring source in the primary flow. They represent the acoustic sources generated at the primary/secondary interface at $r=r_p$ where the density gradients exist. Expressions for corresponding components are obtained from Eqs. (3) by replacing $\rho_s(r_0)$, δ_s, and r_0 by $\rho_p(r_0)$, δ_p, and r_0, respectively, where

$$\delta_p=\frac{\delta(r-r_0)}{r}\delta(z-U_c t)e^{-i\omega t} \tag{5}$$

and

$$\rho_p'(r_0)=\frac{\rho_s-\rho_p}{r_p}St_1,\quad \rho_p''(r_0)=\frac{\rho_s-\rho_p}{r_p^2}St_1^2 \tag{6}$$

Radiation from Sources in the Hot Secondary Stream

While developing the radiation from a cold coaxial flow in Part I, the primary and secondary stream densities were intentionally kept distinctly different, even though when finding the actual radiation for the cold jet we had to make $\rho_p=\rho_s=\rho_f=\rho_0$ all equal to the ambient density. Thus, fundamentally, the radiation expressions found earlier are valid for both hot and cold flows. However, when applying those

fundamental results to a hot flow containing an isolated source, one has to remember that the emergence of additional source terms generated by temperature/density gradients across the fluid interfaces requires that radiation from these extraneous sources must be taken into account. This is an inevitable consequence for a flow where there is a difference in its flow parameters (such as temperature and density) relative to the surrounding fluid. The justification of the structure of these extra sources that result from the gradients across the interfaces and their compatibility with the plug flow acoustic model are explained clearly by Mani.[2]

Since a differentiation of a field due to a simple source representation on the right-hand side of a wave equation with respect to source coordinates yields an appropriate multipole source radiation, one can make use of Eqs. (11) of Part I in Eqs. (3). This will give us the radiation expressions for a quadrupole-type axisymmetric ring source (free from any periodicity n along ϕ) in a hot secondary stream. Thus,

$$a_{11}=\frac{\rho_s\mathcal{K}_s}{i\pi r_s\kappa_0}\left[\left\{\frac{\mathcal{K}_s\kappa_0(C_0-C_2)}{2}-2\left(\frac{\rho_f}{\rho_s}-1\right)\times St_2\frac{\kappa_0}{r_s}\left(C_1+\frac{St_2C_0}{2\mathcal{K}_sr_s}\right)\right\}\cos^2\phi+\left\{C_1-\left(\frac{\rho_f}{\rho_s}-1\right)\frac{St_2C_0}{\mathcal{K}_sr_s}\right\}\sin^2\phi\right]\mathrm{Exp}_1(\mathfrak{R}) \tag{7a}$$

$$a_{22}=\frac{\rho_s\mathcal{K}_s}{i\pi r_s\kappa_0}\left[\left\{\frac{\mathcal{K}_s\kappa_0(C_0-C_2)}{2}-2\left(\frac{\rho_f}{\rho_s}-1\right)\times St_2\frac{\kappa_0}{r_s}\left(C_1+\frac{St_2C_0}{2\mathcal{K}_sr_s}\right)\right\}\sin^2\phi+\left\{C_1-\left(\frac{\rho_f}{\rho_s}-1\right)\frac{St_2C_0}{\mathcal{K}_sr_s}\right\}\cos^2\phi\right]\mathrm{Exp}_1(\mathfrak{R}) \tag{7b}$$

$$a_{33}=\frac{\rho_s}{i\pi r_s}(kc_0/c_f)^2\cos^2\theta C_0\mathrm{Exp}_3(\mathfrak{R}) \tag{7c}$$

$$a_{12}=\frac{\rho_s\mathcal{K}_s}{i\pi r_s\kappa_0}\sin\phi\cos\phi\left[\frac{\mathcal{K}_s\kappa_0(C_0-C_2)}{2}-2\left(\frac{\rho_f}{\rho_s}-1\right)St_2\frac{\kappa_0}{r_s}\left(C_1+\frac{St_2C_0}{2\mathcal{K}_sr_s}\right)-\left\{C_1-\left(\frac{\rho_f}{\rho_s}-1\right)\frac{St_2C_0}{\mathcal{K}_sr_s}\right\}\right]\mathrm{Exp}_1(\mathfrak{R}) \tag{7d}$$

$$a_{13}=\frac{\rho_s}{\pi r_s}kc_0/c_f\cos\theta\cos\phi\left[\mathcal{K}_s\kappa_0C_1+\left(\frac{\rho_f}{\rho_s}-1\right)\frac{St_2C_0}{r_s}\right]\mathrm{Exp}_2(\mathfrak{R}) \tag{7e}$$

$$a_{23}=\frac{\rho_s}{\pi r_s}kc_0/c_f\cos\theta\sin\phi\left[\mathcal{K}_s\kappa_0C_1+\left(\frac{\rho_f}{\rho_s}-1\right)\frac{St_2C_0}{r_s}\right]\mathrm{Exp}_2(\mathfrak{R}) \tag{7f}$$

$$\mathrm{Exp}_n(\mathfrak{R})=\frac{\exp i\{\mathfrak{R}k(c_0/c_f)-wt\}}{\mathfrak{R}[1-(c_0/c_f)(\mathfrak{M}_c-M_f)\cos\theta]^n} \tag{7g}$$

Note that although the above results are valid for a hot jet, we can also derive from them the corresponding results for a cold jet [see Eq. (17) of Part I] simply by letting $\rho_s/\rho_f=1$ in these relations.

Making use of the formulas in Eqs. (15) and (16) of Part I, one can use Eqs. (7) to express the far-field radiation due to a quadrupole-type ring source in the hot secondary stream of a coaxial dual flow as

$$I_{rhs}=\langle\tilde{a}_{33}^2\rangle+2\langle\tilde{a}_{11}^2\rangle+2\langle\tilde{a}_{12}^2\rangle+4\langle\tilde{a}_{13}^2\rangle=\left(\frac{\rho_s}{\pi\mathfrak{R}r_s\kappa_0}\right)\frac{1}{Q_2^2\,|\delta_2|^2}\left\{\frac{|\gamma_0|^2\lambda_{3s}^2(c_0/c_f)^4\cos^4\theta}{Q_2^2\,|M_2|^2}+\left|\frac{3}{4}A_2^2+\frac{3}{4}B_2^2+\frac{A_2B_2}{2}\right|+\frac{1}{4}|A_2-B_2|^2+\frac{2\,|2\gamma_1-B_2|^2\lambda_{3s}^2(c_0/c_f)^2\cos^2\theta}{Q_2^2}\right\} \tag{8a}$$

where

$$A_2=\frac{x_2(\gamma_0-\gamma_2)}{2}-(P_2-1)St_2\left(1+\frac{1}{\sqrt{1+\Sigma}}\right)\left(\gamma_1+\frac{\gamma_0St_2}{2w_2}\right) \tag{8b}$$

$$B_2=\gamma_1-(P_2-1)\frac{\gamma_0St_2}{w_2} \tag{8c}$$

Here again it is interesting to note that by letting $P_2=1$, the hot radiation results of Eqs. (8) can be reduced to the cold radiation results in Eqs. (18) of Part I, when there is an axisymmetric ring source in the secondary stream.

Radiation from Sources in the Hot Primary Stream

Following a similar procedure, one can obtain the radiation expressions for a quadrupole-type axisymmetric ring source (free from any periodicity n along ϕ) in a hot primary stream,

$$b_{11}=\frac{2\rho_pK_p}{i\pi^2r_sr_pr_0}\frac{(A_1\cos^2\phi+B_1\sin^2\phi)}{G_0}\mathrm{Exp}_1(R) \tag{9a}$$

$$b_{22}=\frac{2\rho_pK_p}{i\pi^2r_sr_pr_0}\frac{(A_1\sin^2\phi+B_1\cos^2\phi)}{G_0}\mathrm{Exp}_1(R) \tag{9b}$$

$$b_{33}=\frac{2\rho_p}{i\pi^2r_sr_p}\frac{[k(c_0/c_f)]^2\cos^2\theta}{G_0}J_0(K_pr_0)\mathrm{Exp}_3(R) \tag{9c}$$

$$b_{12}=\frac{2\rho_pK_p}{i\pi^2r_sr_pr_0}\frac{\sin\phi\cos\phi}{G_0}(A_1-B_1)\mathrm{Exp}_1(R) \tag{9d}$$

$$b_{13}=\frac{2\rho_pK_p}{\pi^2r_sr_p}\frac{k(c_0/c_f)\cos\theta\cos\phi}{G_0}[2J_1(K_pr_0)-B_1]\mathrm{Exp}_2(R) \tag{9e}$$

$$b_{23}=\frac{2\rho_pK_p}{\pi^2r_sr_p}\frac{k(c_0/c_f)\cos\theta\sin\phi}{G_0}[2J_1(K_pr_0)-B_1]\mathrm{Exp}_2(R) \tag{9f}$$

$$A_1=\frac{K_pr_0}{2}[J_0(K_pr_0)-J_2(K_pr_0)]-2\left(\frac{\rho_s}{\rho_p}-1\right)\times St_1\frac{r_0}{r_p}J_1(K_pr_0)-\left(\frac{\rho_s}{\rho_p}-1\right)St_1^2\frac{r_0}{r_p}\frac{J_0(K_pr_0)}{K_pr_p} \tag{9g}$$

$$B_1=J_1(K_pr_0)-\left(\frac{\rho_s}{\rho_p}-1\right)St_1\frac{J_0(K_pr_0)}{K_pr_p} \tag{9h}$$

$$\mathrm{Exp}_n(R)=\frac{\exp i\{Rk(c_0/c_f)-\omega t\}}{R[1-(c_0/c_f)(M_c-M_f)\cos\theta]^n} \tag{9i}$$

In the absence of any density gradients across the fluid interface, one can put $\rho_s/\rho_p = 1$ in the preceding equations to derive the radiation for the cold jet.

To find the far-field radiation from the axisymmetric ring source (free from any periodicity along ϕ) in the hot primary stream, Eqs. (15) and (16) of Part I can be used to get

$$I_{rhp} = \langle \bar{b}_{33}^2 \rangle + 2\langle \bar{b}_{11}^2 \rangle + 2\langle \bar{b}_{12}^2 \rangle + 4\langle \bar{b}_{13}^2 \rangle$$

$$= \left(\frac{2\rho_p}{\pi^2 R r_s r_p}\right)^2 \frac{1}{|M_2\delta_1|^2}\left\{\frac{(c_0/c_f)^4\cos^4\theta}{Q_1^2}\left|\frac{J_0(x_1)}{M_1}\right|^2 + \frac{1}{\lambda_{3p}^2}\left|\frac{3}{4}A_1^2 + \frac{3}{4}B_1^2 + \frac{A_1B_1}{2}\right| + \frac{1}{4\lambda_{3p}^2}|A_1 - B_1|^2 + \frac{2(c_0/c_f)^2\cos^2\theta}{Q_1^2}|2J_1(x_1) - B_1|^2\right\} \quad (10a)$$

where we rewrite A_1 and B_1 as

$$A_1 = \frac{x_1}{2}[J_0(x_1) - J_2(x_1)] - \left(\frac{P_1}{P_2} - 1\right) St_1\left[J_1(x_1) + St_1\frac{J_0(x_1)}{2u_1}\right] \quad (10b)$$

$$B_1 = J_1(x_1) - \left(\frac{P_1}{P_2} - 1\right) St_1 \frac{J_0(x_1)}{u_1} \quad (10c)$$

The hot jet radiation in Eqs. (10) can be easily reduced to produce the cold jet radiation in Eqs. (20) of Part I simply by letting $P_1 = P_2 = 1$ in the preceding equations.

Intensity of Radiation due to Ring Sources in Hot Coaxial Dual Flow and Application of the Theory

Since the problem considered here is a linear one, we apply the principle of superposition to combine the intensities of radiation due to the ring sources in both the hot secondary and primary streams of the coaxial flow. Thus, the results of Eqs. (8) and (10) can be combined to obtain the total far-field intensity:

$$I = \left(\frac{\rho_f}{R}\right)^2 \frac{64(1+\Sigma)}{\pi^4 D^4}\left[\frac{RHP}{P_1^2} + \left(\frac{\pi}{1+\sqrt{1+\Sigma}}\right)^2 \frac{RHS}{P_2^2}\right] \quad \text{where} \quad (11a)$$

$$RHP = I_{rhp}\left(\frac{\pi^2 R r_s r_p}{2\rho_p}\right)^2, \quad RHS = I_{rhs}\left(\frac{\pi R r_s t_0}{\rho_s}\right)^2 \quad (11b)$$

Again, to simplify the algebra, we have considered a situation where the centers of the ring sources coalesce to emit radiation which reaches the observer simultaneously. Therefore, $R = \mathcal{R}$ and θ, the angle of emission at the retarded time (measured from the direction of convection), are the same for both. The axial distribution of sources is considered at Strouhal numbers $St_1 = 0.2$ and $St_2 = 0.2$. No attempt is made to model the sources with varying Strouhal numbers.

The change in intensity level is analyzed in the following figures by a plot of intensity level vs θ for various flight Mach numbers M_f. The directional intensity is expressed in terms of the sound pressure level (dB), where

$$\text{dB} = 10\log_{10} I(M_f) \quad (12a)$$

$$I(M_f) = \frac{64}{\pi^4}(1+\Sigma)\left[\frac{RHP}{P_1^2} + \left(\frac{\pi}{1+\sqrt{1+\Sigma}}\right)^2 \frac{RHS}{P_2^2}\right] \quad (12b)$$

The parameters P_1 and P_2 may take on any value to reflect any mode of operation. $P_1 = P_2 = 1$ represents a cold inner/outer mode at an ambient temperature of 288 K; $P_1 = 1$ and $P_2 = 4$ represents an inner cold/outer hot flow at an inner temperature of 288 K and an outer (hot) temperature of 1152 K; $P_1 = 4$ and $P_2 = 1$ represents an inner hot/outer cold flow at an inner (hot) temperature of 1152 K and an outer

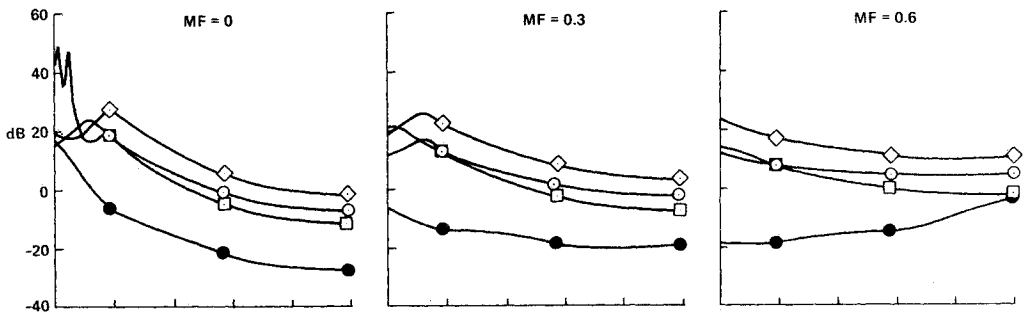

a) Area ratio $\Sigma = 1$, $\bar{M} = 0.48$. •: cold inner-cum-cold outer mode, $M_p = 0.48$, $\Gamma = 1.0$, $P_1 = P_2 = 1$; □: hot inner-cum-hot outer mode, $M_p = 0.95$, $\Gamma = 1.0$, $P_1 = P_2 = 4$; ○: cold inner-cum-hot outer mode, $M_p = 0.5$, $\Gamma = 1.8$, $P_1 = 1$, $P_2 = 4$; ◇: hot inner-cum-cold outer mode, $M_p = 0.9$, $\Gamma = 5/9$, $P_1 = 4$, $P_2 = 1$.

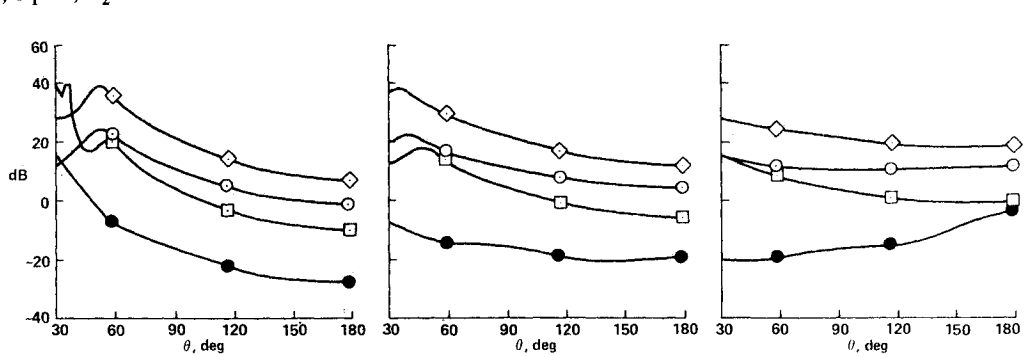

b) Area ratio $\Sigma = 4$, $\bar{M} = 0.46$. •: cold inner-cum-cold outer mode, $M_p = 0.46$, $\Gamma = 1.0$, $P_1 = 1 = P_2$; □: hot inner-cum-hot outer mode, $M_p = 0.92$, $\Gamma = 1.0$, $P_1 = 4 = P_2$; ○: cold inner-cum-hot outer mode, $M_p = 0.5$, $\Gamma = 1.8$, $P_1 = 1$, $P_2 = 4$; ◇: hot inner-cum-cold outer mode, $M_p = 0.84$, $\Gamma = 5/9$, $P_1 = 4$, $P_2 = 1$.

Fig. 1 Change in directional intensity of different coaxial modes at constant thrust and mass flow.

temperature of 288 K. $P_2 = 2$ represents a moderately hot outer flow at a temperature of 576 K.

In Fig. 1, a comparison is made of the variation of intensity levels due to all four possible modes of operation, at outer-to-inner area ratios $\Sigma = 1$ and 4. All of the plots show the variation at higher angles to the jet axis (more than 30 deg) of importance in flight. They indicate that at constant mass flow and thrust, an inner/outer cold mode is the least noisy and an inner hot/outer cold mode is the most noisy. And, in general, from a noise-suppression point of view, an inner/outer cold mode is the most desirable; and, in order of preference, it is followed by an inner/outer hot mode, an inner cold/outer hot mode and, finally an inner hot/outer cold mode. These results agree with the experimental studies of Dosanjh et al.[4] However, one must remember that even though an inner/outer cold mode of operation offers the best noise suppression, it is not the practical engine cycle.

Figure 2 shows the variation of noise when the inner and outer streams are operated at $M_p = 0.5$ and $M_s = 0.9$. This is an inverted-velocity profile jet but under different temperature and thrust conditions. These plots also show that an inner/outer cold stream is not only the least noisy, but also has the maximum thrust and mass flow. An inner hot/outer cold coaxial stream, which has the next to highest thrust, produces the most noise; an inner/outer hot mode produces the minimum thrust, and the inner cold/outer hot mode produces somewhat better thrust, but comparatively more noise. Since the comparisons are meaningful only when the mass flow and thrust are constant, and since the fully cold or fully hot coaxial streams are not very practical engine cycles, let us now turn to those with more relevance to engineering applications.

Figure 3 illustrates the intensity variation when one of the streams is heated. The figures compare the sound pressure levels, SPL (dB), due to three different coaxial combinations: conventional profile (CP), inverted profile (IP), and the variable stream control engine (VSCE) cycles. CP represents a coaxial configuration where the flow pattern consists of a hot, high-speed inner flow combined with a cold, low-speed outer flow. IP is a combination of inverted-velocity and inverted-temperature profiles and represents a coaxial configuration where the flow pattern consists of a cold, low-speed inner flow combined with a hot, high-speed outer flow. The VSCE cycle is obtained from an IP cycle by inverting its outer-to-inner area ratio Σ. Alternately, if the velocity, temperature, and area ratio of a CP cycle are interchanged with its coaxial streams, we will be able to obtain a VSCE cycle as defined above. As a result, the VSCE and CP cycles always maintain the same mass flow and thrust. As area ratios increase from $\Sigma = 1$ to 4, 10, and 20, the IP cycle suffers increased mass loss and increased thrust loss. On the other hand, the mass flow and thrust of the CP cycle (and also a VSCE cycle) increases as the area ratio increases. At $\Sigma = 4$ (and higher), the plots show that the IP cycle provides reduction of noise at all angles, compared to a CP cycle. Also, as one moves from static ($M_f = 0$) to a flight situation, $M_f = 0.3$ or 0.6, the amount of noise reduction already derived in the static case diminishes in the forward quadrant and remains unchanged in the aft quadrant. Furthermore, this loss in the static benefit in the forward quadrant becomes somewhat pronounced as the area ratio and flight velocity increase. These changes occur, however, along with losses in mass flow and thrust in an IP cycle.

On the other hand, a VSCE cycle that maintains a constant mass flow and constant thrust in parity with those of a CP cycle is substantially less noisy than a CP cycle. As shown in Fig. 3b, a VSCE cycle (as compared with a CP cycle) provides a noise reduction of at least 18 dB at $\Sigma = 0.1$, and 30 dB at $\Sigma = 0.05$ (not shown). Furthermore, unlike the IP cycle, this amount of noise reduction is uniformly main-

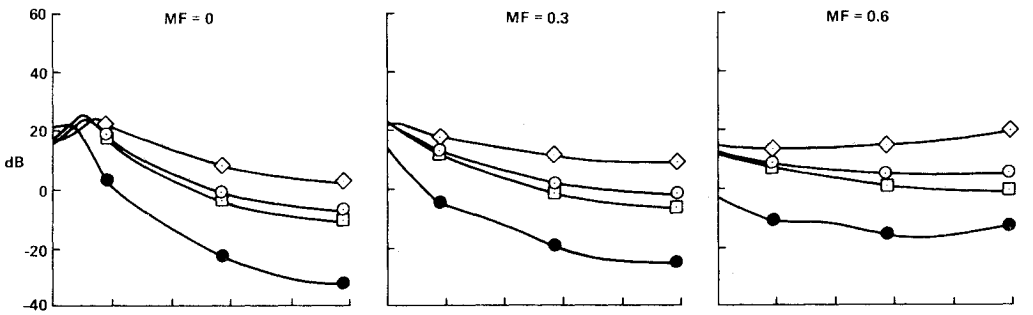

a) Area ratio $\Sigma = 1$. ●: inner cold-cum-outer cold mode, $\bar{M} = 0.73$, $P_1 = 1 = P_2$; □: inner hot-cum-outer hot mode, $\bar{M} = 0.36$, $P_1 = 4 = P_2$; ○: inner cold-cum-outer hot mode, $\bar{M} = 0.48$, $P_1 = 1$, $P_2 = 4$; ◇: inner hot-cum-outer cold mode, $\bar{M} = 0.66$, $P_1 = 4$, $P_2 = 1$.

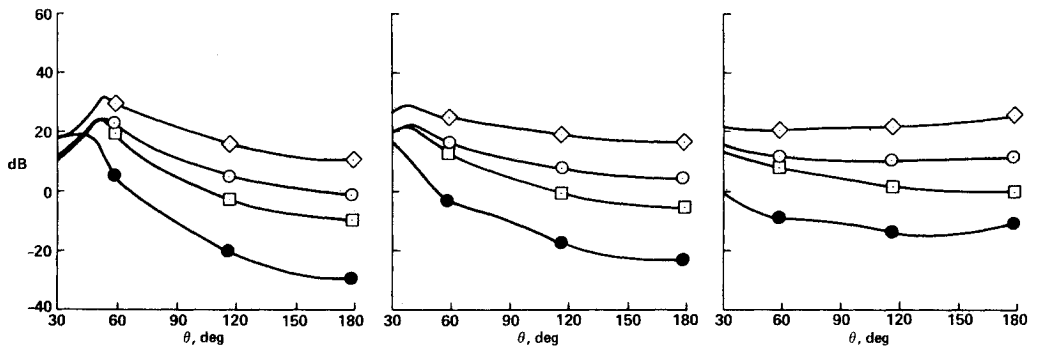

b) Area ratio $\Sigma = 4$. ●: inner cold-cum-outer cold mode, $\bar{M} = 0.84$, $P_1 = 1 = P_2$; □: inner hot-cum-outer hot mode, $\bar{M} = 0.42$, $P_1 = 4 = P_2$; ○: inner cold-cum-outer hot mode, $\bar{M} = 0.46$, $P_1 = 1$, $P_2 = 4$; ◇: inner hot-cum-outer cold mode, $\bar{M} = 0.81$, $P_1 = 4$, $P_2 = 1$.

Fig. 2 Change in directional intensity of different coaxial modes at variable thrust and mass flow, and with constant $M_p = 0.5$, $\Gamma = 1.8$.

tained at all angles around the jet both statically and in flight. It should be noted that, as the values of Σ go from 0.25 to 0.1 to 0.05, the net mass flow and thrust continue to increase. Thus, if the CP cycle is interchanged with a VSCE cycle, we not only maintain the same mass flow and thrust, we also obtain a tremendous noise reduction at all angles and all situations—both statically and in flight. Thus, it is clear that a VSCE cycle is the best engine cycle of all coaxial configurations conceived herein and will provide the quietest nozzle possible.

Figure 4 illustrates the change in directional intensity as a result of flight relative to the static case, $M_f = 0$. The plots show that the flight effects induce reduction of noise in the aft quadrant and amplification of noise in the forward quadrant. The coalescence of all of the static and flight curves at one point implies that there are absolutely no effects due to flight at $\theta = 90$ deg to the jet axis. These flight effects occur at all values of outer-to-inner area ratios Σ. Moreover, as Σ increases, the noise level at all angles is enhanced both statically as well as in flight.

Figure 5 shows the change in directional intensity of radiation due to an inverted-profile coaxial flow, as a result of variation in outer-to-inner area ratios (Σ) and as a result of flight. As flight Mach number M_f increases, the parts of the curves in the aft quadrant gradually decrease and those in the forward quadrant gradually increase. Furthermore, as the outer-to-inner area ratios Σ increase, a moderate noise increase occurs at all angles. They also indicate that the intensity is directional with a peak more or less close to the jet axis. As the area ratio (Σ) increases, the directivity becomes more pronounced and the peak location occurs closer to the exhaust axis. The static amplification of noise at the peak angle relative to that at $\theta = 90$ deg is about 10 dB for $\Sigma = 10$, 20, 40, 80, and about 13 dB for $\Sigma = 4$, and about 18.5 dB for

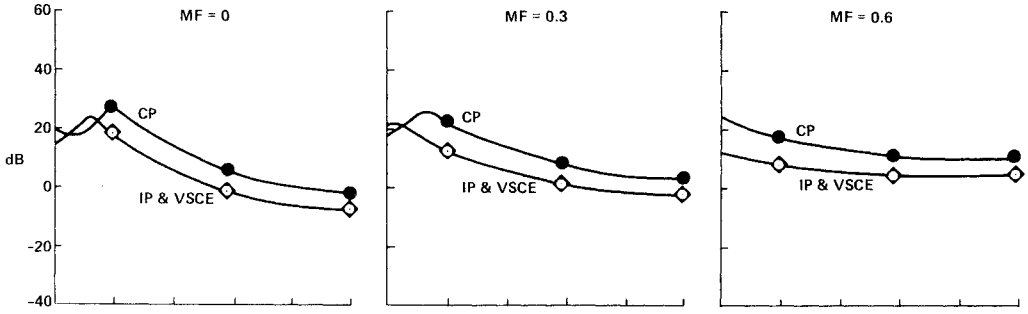

Fig. 3a Comparison of SPL due to conventional profile (CP), inverted profile (IP), and variable stream control engine (VSCE) cycles, all having the same mass flow and thrust; area ratio $\Sigma = 1$. CP (●): $M_p = 0.9$, $\Sigma = 1$, $\Gamma = 5/9$, $P_1 = 4$, $P_2 = 1$, $\bar{M} = 0.48$; IP (○): $M_p = 0.5$, $\Sigma = 1$, $\Gamma = 1.8$, $P_1 = 1$, $P_2 = 4$, $\bar{M} = 0.48$; VSCE (◇): $M_p = 0.5$, $\Sigma = 1$, $\Gamma = 1.8$, $P_1 = 1$, $P_2 = 4$, $\bar{M} = 0.48$.

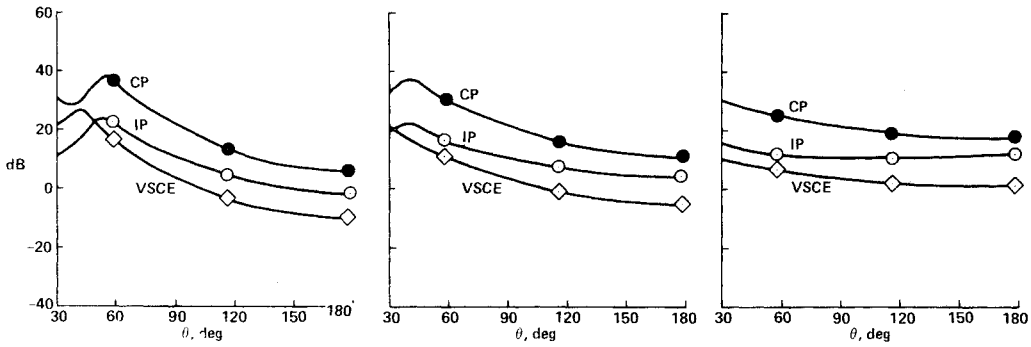

Fig. 3b Comparison of SPL due to conventional profile (CP), inverted profile (IP), and variable stream control engine (VSCE) cycles, with only CP and VSCE cycles having the same mass flow and thrust; area ratio $\Sigma = 4$. CP (●): $M_p = 0.9$, $\Sigma = 4$, $\Gamma = 5/9$, $P_1 = 4$, $P_2 = 1$, $\bar{M} = 0.49$; IP (○): $M_p = 0.5$, $\Sigma = 4$, $\Gamma = 1.8$, $P_1 = 1$, $P_2 = 4$, $\bar{M} = 0.46$; VSCE (◇): $M_p = 0.5$, $\Sigma = 0.25$, $\Gamma = 1.8$, $P_1 = 1$, $P_2 = 4$, $\bar{M} = 0.49$.

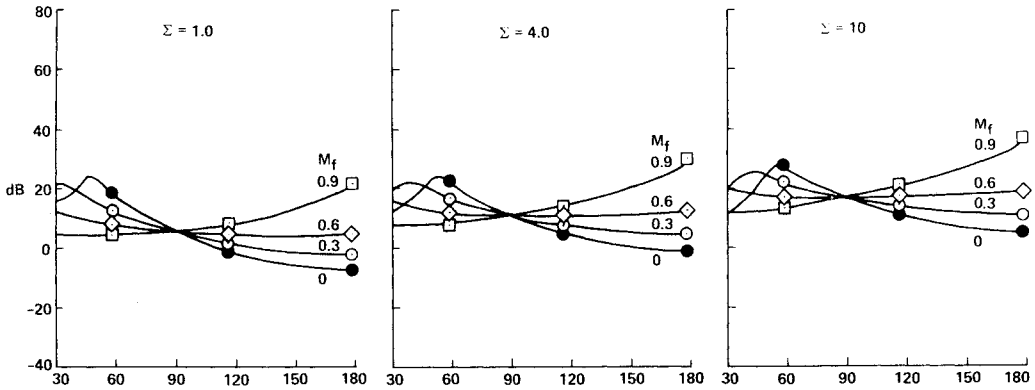

Fig. 4 Change in directional intensity as a result of flight. $M_p = 0.5$, $\Gamma = 1.8$, $P_1 = 1$, $P_2 = 4$, $\bar{M} = 0.48$.

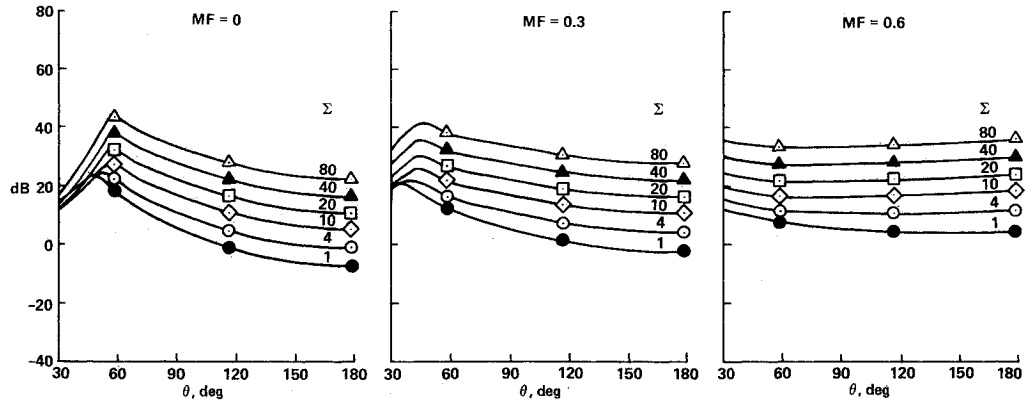

Fig. 5 Change in directional intensity and comparison of SPL of an inverted profile as a result of varying outer-to-inner area ratio (Σ): $M_p = 0.5$, $\Gamma = 1.8$, $P_1 = 1$, $P_2 = 4$. ●: $\Sigma = 1$, $\bar{M} = 0.476$; ○: $\Sigma = 4$, $\bar{M} = 0.460$; ◇: $\Sigma = 10$, $\bar{M} = 0.455$; □: $\Sigma = 20$, $\bar{M} = 0.453$; ▲: $\Sigma = 40$, $\bar{M} = 0.4513$; △: $\Sigma = 80$, $\bar{M} = 0.4510$.

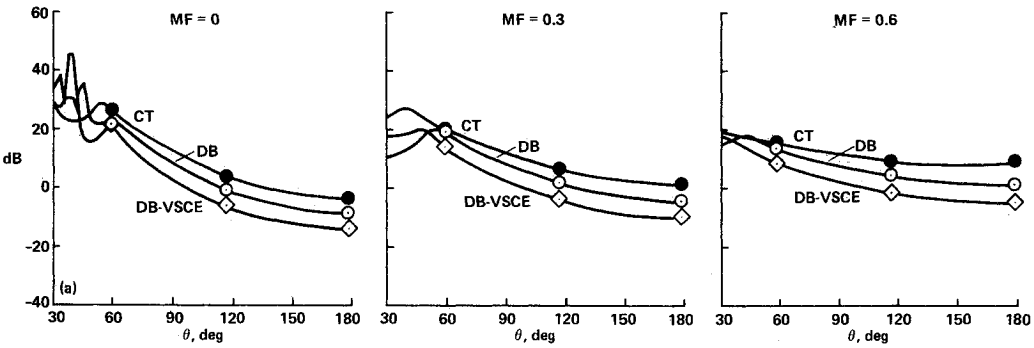

a) Area ratio $\Sigma = 4$. CT (●): $M_p = 0.9$, $\Sigma = 4$, $\Gamma = 0.6$, $P_1 = 4$, $P_2 = 2$, $\bar{M} = 0.40$; DB (○): $M_p = 0.9$, $\Sigma = 4$, $\Gamma = 1.2$, $P_1 = 2$, $P_2 = 4$, $\bar{M} = 0.56$; DB-VSCE (◇): $M_p = 0.9$, $\Sigma = 0.25$, $\Gamma = 1.2$, $P_1 = 2$, $P_2 = 4$, $\bar{M} = 0.62$.

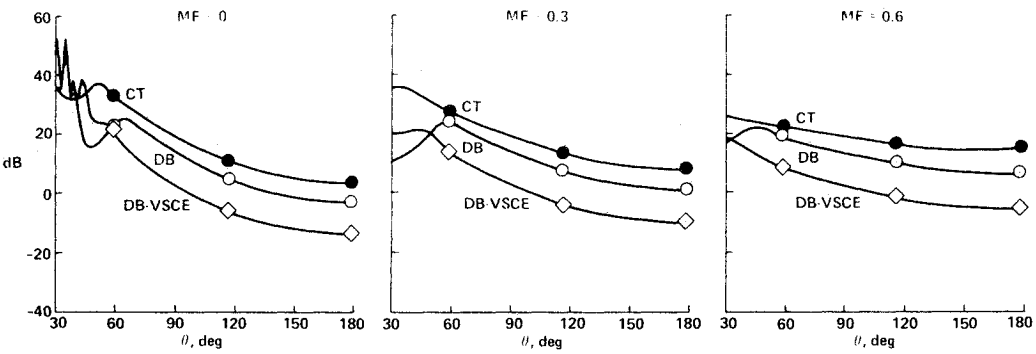

b) Area ratio $\Sigma = 10$. CT (●): $M_p = 0.9$, $\Sigma = 10$, $\Gamma = 0.6$, $P_1 = 4$, $P_2 = 2$, $\bar{M} = 0.389$; DB (○): $M_p = 0.9$, $\Sigma = 10$, $\Gamma = 1.2$, $P_1 = 2$, $P_2 = 4$, $\bar{M} = 0.55$; DB-VSCE (◇): $M_p = 0.9$, $\Sigma = 0.1$, $\Gamma = 1.2$, $P_1 = 2$, $P_2 = 4$, $\bar{M} = 0.628$.

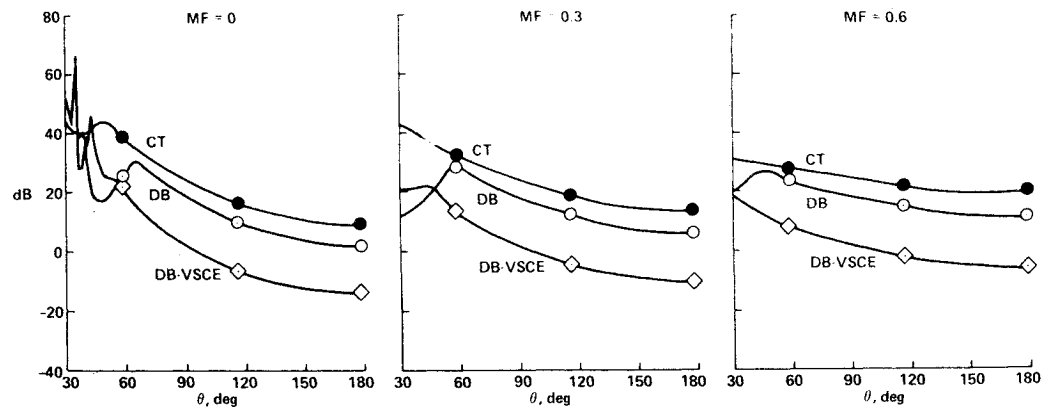

c) Area ratio $\Sigma = 20$. CT (●): $M_p = 0.9$, $\Sigma = 20$, $\Gamma = 0.6$, $P_1 = 4$, $P_2 = 2$, $\bar{M} = 0.385$; DB (○): $M_p = 0.9$, $\Sigma = 20$, $\Gamma = 1.2$, $P_1 = 2$, $P_2 = 4$, $\bar{M} = 0.54$; DB-VSCE (◇): $M_p = 0.9$, $\Sigma = 0.05$, $\Gamma = 1.2$, $P_1 = 2$, $P_2 = 4$, $\bar{M} = 0.632$.

Fig. 6 Comparison of SPL due to conventional turbofan (CT) cycle, duct-burning (DB) cycle, and duct-burning-cum-variable stream control engine (DB-VSCE) cycle.

$\Sigma = 1$. These differences in peak SPL decrease as the flight Mach number M_f increases.

Figure 6 shows the change in directional intensity and the variation in sound pressure level, SPL (dB), due to coaxial streams where both of the streams are unequally heated. These coaxial configurations are: conventional turbofan (CT) profile, duct-burning (DB) profile, and duct-burning-cum-variable stream control engine (DB-VSCE) cycle. CT represents a coaxial configuration where the flow pattern consists of a very hot, high-speed inner flow combined with a hot, low-speed outer flow. DB represents a coaxial configuration where the flow pattern consists of a hot, low-speed inner flow combined with a very hot, high-speed outer flow. A DB-VSCE cycle is obtained from a DB cycle by inverting its outer-to-inner area ratio Σ. Among three different cycles considered here, a DB-VSCE cycle is the least noisy and has the maximum mass flow and thrust. On the other hand, a CT cycle is the most noisy even though it has the least mass flow and thrust. Figure 6b shows that at area ratio $\Sigma = 10$ and flight Mach number $M_f = 0$, the noise reduction for the DB-VSCE cycle relative to a CT cycle is at least 11.5 dB in the aft quadrant and 17.5 dB in the forward quadrant. This noise reduction is increased to at least 14 dB in the aft quadrant and 18 dB in the forward quadrant due to flight at $M_f = 0.3$. As the flight Mach number is further increased to $M_f = 0.6$, the aft-quadrant noise reduction remains more or less stable, but in the forward quadrant the noise reduction is increased to nearly 20 dB. At $\Sigma = 20$, shown in Fig. 6c, noise reductions due to a DB-VSCE cycle, relative to a CT cycle, are further enhanced at all angles both statically and in flight. These occurrences take place at high mass flow and thrust conditions. Thus, it is clear that among the three possible engine cycles, where both coaxial streams are unequally heated—CT, DB, and DB-VSCE cycles—a DB-VSCE cycle has not only the maximum mass flow and thrust, but also the least noise both statically and in flight. And the benefit in noise reduction is systematically maintained and markedly enhanced at all angles as the outer-to-inner area ratio increases.

Summary

The effects of flight on noise from hot coaxial flows have been studied based on a double vortex-sheet flow model. The following conclusions have been reached based on the specific assumptions and calculations introduced herein. Accordingly, as a result of this sutdy, it has been found that the effects of flight on noise from heated coaxial dual flow induce: 1) amplification of noise in the forward quadrant ($\pi/2 \le \theta \le \pi$); 2) reduction of noise in the aft quadrant ($0 \le \theta \le \pi/2$); and 3) absolutely no impact on noise at $\theta = 90$ deg to the jet axis.

Furthermore, the results of this study indicate the following.

1) Among all of the possible coaxial configurations where one of the streams is heated, namely, the conventional profile (CP), inverted profile (IP), and variable stream control engine (VSCE) cycle, a VSCE cycle (Fig. 3) is the best engine cycle insofar as it provides a tremendous noise reduction, with respect to the CP and IP cycles, both statically and in flight, while maintaining the same mass flow and thrust as a CP cycle.

2) The noise reduction of a VSCE cycle relative to a CP cycle dramatically increases from approximately 18 dB at (an outer-to-inner area ratio) $\Sigma = 0.25$ to 25 dB at $\Sigma = 0.1$, and to 30 dB at $\Sigma = 0.05$ at all angles.

3) The noise suppression due to the VSCE cycle is uniformly maintained at all static and flight conditions.

4) Among all of the possible coaxial configurations (Fig. 6) where both the streams are unequally heated, namely, the conventional turbofan (CT) cycle, duct-burning (DB) cycle, and duct-burning-cum-variable stream control engine (DB-VSCE) cycle, a DB-VSCE cycle provides the maximum mass flow and thrust and, at the same time, it is the least noisy.

5) The static benefit in noise reduction due to a DB-VSCE cycle over a CT cycle is of the order of 5.6-10 dB at $\Sigma = 0.25$, 11-17.5 dB at $\Sigma = 0.1$, and 17.5-22.5 dB at $\Sigma = 0.05$; the lower dB levels ranging over the aft quadrant and the higher dB levels ranging over the forward quadrant.

Concluding Remarks

The coaxial jet noise problem has been discussed on the basis of a double vortex-sheet flow model which involves deliberate suppression of inherent instabilities of the flow. The analysis reveals many important features consistent with the familiarly known results of coaxial jet noise.

One of the most striking features obtained as a result of this study is that, when both streams of a coaxial flow are unequally heated, a duct-burning profile combined with a variable stream control engine (DB-VSCE) concept is the most powerful engine cycle and provides the maximum mass flow and thrust and yet generates the minimum noise both statically and in flight. Thus, in the author's opinion, this coaxial engine cycle possibly holds the key to the search for the most effective nozzle needed to usher us into an era of quiet aircraft.

Acknowledgments

This study was conducted as part of a NASA Ames program of research into flight effects on jet noise under NASA Cooperative Agreement Contract NCC 2-75. I am thankful to David H. Hickey and Adolph Atencio Jr. of NASA Ames for their useful discussion and helpful suggestions. Thanks are also given to R. Mani of General Electric Co., T. F. Balsa of the University of Arizona, and K. Karamcheti of Stanford for their interest in this work, and to Yen Liu of Stanford University for his invaluable assistance in programming these calculations. I also express my appreciation to all of my referees, H. K. Tanna of Lockheed Advanced Aeronautics, and Paul Soderman of NASA Ames, for their useful suggestions and comments which have helped the author to present the paper in the above form.

References

[1]Mani, R., "The Influence of Jet Flow on Jet Noise. Part 1. The Noise of Unheated Jets," *Journal of Fluid Mechanics*, Vol. 73, Pt. 4, 1976, pp. 753-778.

[2]Mani, R., "The Influence of Jet Flow on Jet Noise. Part 2. The Noise of Heated Jets," *Journal of Fluid Mechanics*, Vol. 73, Pt. 4, 1976, pp. 779-793.

[3]Hoskins, R. F., *Generalized Functions*, John Wiley & Sons, New York, 1979.

[4]Dosanjh, D. S., Bhutiani, P. K., Ahuja, K. K., and Bassiouni, M. R., "Supersonic Jet Noise Suppression by Coaxial Cold/Heat Jet Flows," AIAA Paper 76-507, 1976.

[5]Dash, R., "Flight Effects on Noise from Coaxial Dual Flow, Part I: Unheated Jets," *AIAA Journal*, Vol. 24, May 1986, pp. 761-769.